Phase Topology and Percolation in Two-Component Lipid Bilayers: A Monte Carlo Approach

Fernando P. Coelho,* Winchil L. C. Vaz,# and Eurico Melo*
*Instituto de Tecnologia Química e Biológica and IST, Apartado 127, P-2780 Oeiras, and #Unidade de Ciências Exactas e Humanas, Universidade do Algarve, Campus de Gambelas, P-8000 Faro, Portugal

ABSTRACT Monte Carlo simulations of fluorescence recovery after photobleaching (FRAP) experiments on two-component lipid bilayers systems in the solid-fluid phase coexistence region were carried out to study the geometry and size of fluid domains in these bilayers. The gel phase was simulated by superposable elliptical domains, which were either of predetermined dimensions, increasing in number with increasing gel phase fraction, or of predetermined number, increasing in dimensions with increasing gel phase fraction. The simulations were done from two perspectives: 1) a time-independent analysis of fractional fluorescence recovery as a function of fractional fluid phase in the system; and 2) a time-dependent analysis of fractional fluorescence recovery as a function of time at a given fraction of fluid phase in the system. The time-dependent simulations result in recovery curves that are directly comparable to experimental FRAP curves and provide topological and geometrical models for the coexisting phases that are consistent with the experimental result.

INTRODUCTION

Phospholipid bilayers composed of binary lipid mixtures form nonideal mixtures that exhibit phase separation over a large range of temperatures at constant pressure (Shimshick and McConnell, 1973; Wu and McConnell, 1975; Mabrey and Sturtevant, 1976). We will be concerned here with rigid and fluid coexisting phases, but two different liquid phases may as well be simultaneously present in a bilayer (Almeida et al., 1992a). These two phases form a mosaic of microscopic phase domains whose long-term stability, although controversial from the theoretical viewpoint (Mouritsen and Jørgensen, 1994), has been observed experimentally (Vaz et al., 1989). An important question concerning the bilayer structure in the region of phase coexistence concerns the topology of the phases in equilibrium. Notably, the lateral organization of the domains in each phase of a bilayer in this physical state may control the kinetics and yield of chemical processes occurring between membrane components (Melo et al., 1992). These components must percolate toward each other to allow collisional interaction. Therefore, when because of physical or chemical conditions a phase separation is developed in the membrane, the possibility and characteristics of the molecular percolation become important reaction parameters (Melo et al., 1992; Vaz, 1992; Vaz and Almeida, 1993).

For a given composition, by decreasing the temperature from above to below the liquidus line, the formation of the gel phase will take place at the cost of the fluid (the system enters the two-phase solid-liquid coexistence region). In the initially completely homogeneous liquid phase, isolated solid domains appear at some nucleation points as a minute fraction of the total mass. As the temperature is decreased, more gel phase is induced to form. A given phase is considered to be percolating when a continuous cluster of its domains allows the tracing of a path across the entire system without leaving this phase (Stauffer and Aharony, 1994). Therefore, even if some regions of fluid may be, at this stage, isolated from the bulk fluid fraction, at least part of it is continuous and the system is still defined as percolating. Extrapolating what is observed in Langmuir-Blodgett films to our system, the increase in the fractional mass of solid may occur via the growth of the existing rigid domains without changing the number of domains, or by nucleating new domains, or both (Markov, 1995). In any case, as we approach the solidus line, for a given composition, percolation in the fluid phase is lost and the solid becomes continuous over larger distances. The fluid fraction at which the liquid phase becomes disconnected is known as the percolation threshold, p_c (Stauffer and Aharony, 1994; Saxton, 1987).

The percolation threshold defines an important inflection point in the kinetics and the yield of reactions between those membrane proteins and/or other reactant species essentially insoluble in solid phases (Melo et al., 1992). Whereas below the percolation threshold their diffusion will be confined to isolated liquid domains of heterogeneous geometry and area, immediately above the percolation point the number of available reactants per domain increases rapidly, although their free diffusion in the membrane plane is still restricted by the rigid domains. These facts may have consequences at various levels for the biological processes in a membrane because of the forced reactant isolation or the hindrance of their diffusion (Vaz, 1996). In fact, it is the topology of the coexisting phases that, in this case, conditions the rate and the chemical yield of the biochemical processes.

To try to understand and model the consequences of phase separation in the reactions occurring in the mem-

Received for publication 28 October 1996 and in final form 10 January 1997.

Address reprint requests to Dr. Eurico Melo, Instituto de Tecnologia, Química e Biológica, Apartado 127, P-2780 Oeiras, Portugal. Tel.: 351-1-441-7823; Fax: 351-1-442-1161; E-mail: eurico@itqb.unl.pt.

0006-3495/97/04/1501/11 $2.00

branes, especially from the kinetic viewpoint, it is essential to have information concerning the structure and dimensions of the phase-separated domains. However, the pattern of the fluid and gel domains in a membrane has never been directly observable by conventional optical microscopy, presumably because the dimension of the domains falls below the resolution of the technique ($\sim\lambda/2$). Therefore, if we want to access the topology of the phase-separated membrane, either a better resolution is needed, or indirect methods must be employed. Some high-resolution techniques such as electron microscopy (Hui, 1981), atomic force microscopy (Radmacher et al., 1992), and near-field scanning optical microscopy (Hwang et al., 1995) have been used with varying success, and we will have to await refinements before their utility can be clearly assessed. The objective of the present work is to discuss possible geometrical arrangements of the fluid-rigid mosaic that are compatible with the experimental findings concerning molecular diffusion in these systems obtained from the fluorescence recovery after photobleaching (FRAP) technique.

Vaz et al. (1989) showed for the first time how the FRAP technique could be used to determine the percolation threshold in phospholipid bilayers. In that work the diffusion of a fluorescent tracer molecule, only soluble in the fluid phase of a two-phase fluid-solid coexistence system, was studied, and this made it possible to draw some conclusions regarding in-plane percolation in these membranes. Since then several systems have been studied with the same method (Vaz et al., 1990; Bultmann et al., 1991; Almeida et al., 1992b).

In a FRAP experiment, if free diffusion occurs over the entire area of the membrane being examined, and the illuminated area is only a very small fraction of the total membrane area, the measured fluorescence intensity at "infinite" time after the photobleaching pulse attains the value measured before the pulse. Incomplete fluorescence recovery is symptomatic of immobilization of the fluorescent probes in the membrane plane during the time of the experiment. If the fluid-phase domains are of a size comparable to the photobleached area, a sharp change in the recovery fraction at the percolation threshold is not observed. Instead, if we represent the fraction of fluorescence recovery as a function of the fraction of area of the fluid phase for a given phase-separated phospholipid system, we obtain a sigmoid curve. Assuming that the FRAP fractional fluorescence recovery represents the probability of percolation of the liquid phase in the membrane under investigation, Almeida et al. (1992b, 1993) concluded that the system percolation threshold should be defined by the inflection point of the curve.

If the diffusion in the phase-separated lipid bilayer is viewed as a problem of continuum percolation in two dimensions, the percolation threshold, defined as the minimum liquid area fraction for which this phase is still continuous, can give an insight into the shape of the solid-phase domains (Xia and Thorpe, 1988). However, to be able to characterize its topology within the context of the existing continuum percolation theory, an a priori definition of the geometric elements with which the rigid phase is build becomes necessary. One possible model representing the gel-phase elements as ellipses with aspect ratio b/a has been thoroughly studied by Xia and Thorpe (1988) and will be designated hereafter as the fixed-ellipse model. Within the context of this model, the solid domain structure would be characterized by a random distribution of identical ellipses that may superimpose in each bilayer sheet. Differences in the gel-phase fraction arise from varying the number of ellipses per unit of membrane area without changing the geometric characteristics of the ellipses. It is important to recall that, as Xia et al. have demonstrated, the percolation threshold, p_c, is a function of the ellipse aspect ratio, b/a, and so, for a given experimental p_c value it will be possible to estimate b/a. Besides, this relation between p_c and b/a being highly convenient, the use of ellipses is quite reasonable, at least when the fraction of solid phase is small, because in monolayers the crystalline domains present an ellipse-like shape (Keller et al., 1987). Although this treatment allows an estimation of the solid-domain shape, it does not give any clue concerning its absolute size or the shape and size of the coexistent fluid domains.

In an attempt to evaluate the average size of the phase-separated domains, Almeida et al. (1993) have deduced a relationship between the fractional recovery of fluorescence at equilibrium after photobleaching, the fractional area of the fluid phase, and the ratio between the linear dimension of the fluid domains and the radius of the FRAP bleaching spot. This treatment presupposes that it is possible to derive the exact value of the fractional fluorescence recovery at equilibrium after photobleaching from the experimental curves.

In this work we present a Monte Carlo simulation of the percolation problem in biphasic (solid-fluid coexistence) lipid bilayers. We have used the fixed-ellipse model, referred to above, in these simulations. A first phase of this work attempted to reproduce experimental plots of fractional fluorescence recovery at equilibrium after photobleaching versus fluid fraction of the system. Agreement of the simulations with the experimental points was obtained at values above the percolation threshold of the system with significant discrepancy close to or below the percolation threshold. This suggested that the dimensions of the fluid domains relative to the radius of the FRAP spot were reasonably well estimated by the model.

In a second phase of this work we attempted to understand the discrepancy between the model-derived simulations and the experimental results. The experimental values of the fractional fluorescence recovery are essentially a result of interpretation of the raw data, and it may be argued that a better procedure would be to simulate the complete experimental curves in the time domain. In practice, the experimental recovery curves in the region of phase coexistence cannot be fitted with the normal solution of the equation for homogeneous diffusion in two dimensions, as derived by Axelrod et al. (1976) or Soumpasis (1983),

because they exhibit an anomalous tail in the long-time regime just above and below the percolation threshold. In previous work, to obtain a good fit, we artificially added a "linear ramp" to the conventional solution expression (Vaz et al., 1989, 1990; Bultmann et al., 1991; Almeida et al., 1992b). This artifice was based on the interpretation that the slow diffusion component was due to tracer diffusion in the gel-phase defects, with a recovery time that was slow on the time scale of our FRAP experiment, thus permitting approximate description by a straight line superimposed on the fluid diffusion component. The extremely good fits obtained (an example of which is presented in Fig. 1) do not dismiss other interpretations, including one in which the slow component is inherent to diffusion with percolation.

An alternative analysis of the FRAP experimental data can be achieved by utilization of the fixed-ellipse model in a Monte Carlo simulation in the time regime. Within the context of the continuum percolation model, the simulated FRAP curves are obtained, assuming that the lateral diffusion of the tracer molecules in the FRAP experiment can be treated as a random walk on a two-dimensional obstructed continuum. The impenetrable obstacles may be represented by random inclusion of superimposable elliptical structures of uniform area, as described earlier. The fit of the simulation results to the experimental time-resolved FRAP curves should then provide the ideal domain geometry and dimensions within the context of the model. This procedure, with which only diffusion of the probe in the liquid phase is reported, can be used to verify whether the referred long time tail is actually associated with diffusion in gel defects or whether it is related to an anomalous diffusion in a percolating system.

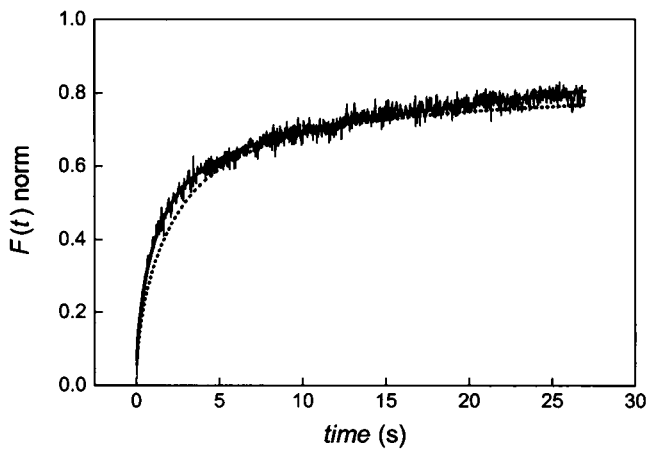

FIGURE 1 Fit of experimental time-dependent FRAP recovery data for the DMPC/DSPC (50/50) system at 34.9°C, $p = 0.47$ (*noisy curve*) (Vaz et al., 1989). The smooth curves represent best fits to the experimental data, using the expression derived by Soumpasis (1983) with and without adding a "linear ramp" (*solid and dotted lines*, respectively). In the first case the best fit was obtained with fitting parameters $\tau_D = 1.02$ s, $F(0) = 2904$ counts, $F(\infty) = 6560$ counts, slope of "linear ramp" = 21.3 counts/s, and the goodness-of-fit parameter $\chi^2 = 1.3$. For the second case the parameters are $\tau_D = 1.99$, $F(0) = 3238$ counts, $F(\infty) = 7151$ counts, and $\chi^2 = 1.9$. All curves are normalized.

Fluid- and solid-domain topologies being complementary, from the above simulations we obtain the necessary information about the geometry of the fluid domains near or below the percolation threshold, a region where such information may be of fundamental biological interest, particularly with respect to molecular interactions between diffusing reactants (Melo et al., 1992).

We are not the first to attempt an evaluation of the average domain sizes in bilayers constituted of mixed phospholipids. A first attempt has been presented by Sankaram et al. (1992) for mixed 1,2-dimyristoyl-*sn*-glycero-(3)-phosphocholine (DMPC)/1,2-distearoyl-*sn*-glycero-(3)-phosphocholine (DSPC) bilayers. From an electron spin resonance study these authors conclude that the disconnected liquid crystalline domains are on the order of several hundred lipid molecules, although they admit that larger domains are possible (Sankaram et al., 1992). In a computer simulation of FRAP experiments, Schram et al. (1994) estimated the domain size of the fluid domains in the plasma membrane of human fibroplasts as having a ~0.4-μm radius. Still smaller sizes, around 100 molecules, where proposed by Mendelson et al. (1995) and Snyder et al. (1995), based in isotope infrared spectroscopic studies. In the Results and Discussion sections we will compare these values with those that derive from our simulations.

METHODS

FRAP experimental data

The experimental data with which our simulations are compared pertain to the DMPC/DSPC mixed lipid system and refer only to the equimolar mixture. Details of the experimental set-up and procedure have been given previously (Vaz et al., 1989). It is relevant, however, to recall that the radius of the bleaching spot used in these experiments is 3 μm, and that the fluorescent probe molecule, *N*-(7-nitrobenz-2-oxa-1,3-diazol-4-yl)-1,2-dilauroyl-*sn*-glycero-3-phosphoethanolamine (NBD-DLPE), partitions almost exclusively in the fluid phase. In the present work all of the analysis was performed on the curves obtained during the heating scans because those presented less scatter, with at least two experimental files being averaged for each temperature.

The fluorescence fractional recovery values R are obtained from the fluorescence intensity before photobleaching, $F(t < 0)$, the fluorescence intensity at infinite time after photobleaching, $F(\infty)$, and the fluorescence intensity at zero time, $F(0)$. Whereas $F(t < 0)$ is directly obtained by averaging the fluorescence of the sample before the bleaching pulse, $F(\infty)$ and $F(0)$ are computed by fitting the time-dependent recovery curves, $F(t)$, to the Soumpasis equation for the recovery after photobleaching a uniform circular spot, to which a linear time ramp is added when necessary to "fit" the slow component, as described elsewhere (Vaz et al., 1989, 1990; Bultmann et al., 1991; Almeida et al., 1992b). Fig. 1 shows a typical recovery curve with its fit. A recovery time constant τ is also obtained, but its precise physical meaning will be discussed later in this work.

Area fraction of the coexisting phases

To simulate the phase-separated single bilayer in which the fluorescence recovery after photobleaching events will take place, knowledge of the area fractions of coexisting liquid and solid phases at a given temperature is essential. The phase diagram of Mabrey and Sturtevant (1976) was used to obtain the mass fraction of the two coexisting phases at any given temperature. Several authors disagree over some fundamental aspects of this

phase diagram (Knoll et al., 1981; Luna and McConnell, 1978), but for an equimolar mixture, all of the published diagrams give, for our purposes, identical results. The mass fraction values were further converted to the corresponding area fractions, assuming that the area per phospholipid molecule is 45 Å^2 in the gel (Wiener et al., 1989) and 63 Å^2 in the fluid phase (Almeida et al., 1993).

Fractional recovery simulations

All of the computer simulations of the FRAP experiments were carried out on a 486/66 MHz IBM-compatible PC using MS FORTRAN Powerstation v1.00. The phospholipid bilayers are represented as two-dimensional arrays stored as one-dimensional vectors to speed up the memory access time. To save memory and consequently to allow larger bilayer planes to be simulated, the memory storage was made on a bit basis. A library pseudo-random number generator was used: routine RAN1 from the Numerical Recipes FORTRAN library (Press et al., 1989).

For the fixed-ellipse model with aspect ratio b/a, where b and a are, respectively, the semi-minor and semi-major axes of the ellipse, the area fraction occupied by the solid domains, c, is attained by adding the necessary number of identical ellipses. Each ellipse is added to the matrix simulating the bilayer at a random position defined by the coordinates of its center and with a random orientation of the a axis. The ellipses are free to superimpose, and the number of ellipses needed to obtain a defined solid area fraction, c, is computed by Eq. 1, derived by Xia et al., which relates the fluid area fraction, $p = 1 - c$, to the number of solid ellipses:

$$p = e^{(-A\rho)}, \tag{1}$$

where $A = \pi ab$ is the area of each ellipse, and ρ is the number of ellipses per unit of membrane area.

The FRAP bleaching spot is represented by a circular observation area centered in each plane with a radius equivalent to 3 μm. The fluorescence recovery at equilibrium is determined by computing both the area fraction of closed fluid pools totally contained inside the spot whose fluorescence is unrecoverable (internal domains), and the area fraction of those that expand outside of the bleaching beam and are partially recoverable (peripheric domains). In a real FRAP experiment the bleaching beam intersects a stack of a few hundred bilayers; hence the observed fractional fluorescence recovery R is an average value. By averaging the results from several simulated bilayers, we get a result that can be compared with the experimental observation:

$$R = \frac{\sum_j^{N_L} \sum_l^{N_P} [(A_R)_{jl} - ((A_R)_{ij}^2/(A_D)_{jl})]}{\sum_j^{N_L} [\sum_k^{N_I} (A_I)_{jk} + \sum_l^{N_P} (A_R)_{jl}]}. \tag{2}$$

In Eq. 2 N_L is the total number of bilayers simulated, N_P the number of peripheral domains, $(A_D)_{jl}$ the area of the peripheral fluid domains l inside the spot in the bilayer sheet j, $(A_R)_{jl}$ the total area of the peripheral fluid domains l in the bilayer sheet j, and $(A_I)_{jk}$ the total area of the internal fluid domains k inside the spot in the bilayer sheet j.

The counting and area sizing of the fluid domains remaining in the bilayer plane after the placement of ellipses and intersecting the bleaching spot were done with the version of the Hoshen and Kopelman algorithm presented by Stauffer and Aharony (1994).

For a given ellipse size and aspect ratio, the simulated recovery plot was then constructed by increasing the solid area fractions in each matrix, by computing the corresponding fractional recovery, and finally by accumulating the successive results for each bilayer sheet.

Because we are dealing with a continuum percolation problem, we needed to use a matrix resolution such that the site percolation method, implicit when we use a discrete matrix, may describe with good approximation the continuum process. The criteria behind the definition of the necessary resolution are related to the resolution needed to allow the construction in the matrix plane of ellipses with an area close to the corresponding analytical one ($A = \pi ab$). It was empirically verified, at least for the various geometries explored, that with a resolution r (lattice spacing 47 μm), given by Eq. 3, the area of the digital image of an ellipse is identical to the real object area within an error of ±3%:

$$r = \frac{10}{(a + b)/2}. \tag{3}$$

For domains with $(a + b)/2 = 1$ μm, each lattice site contains about 10^4 phospholipid molecules.

The number of bilayers simulated for a given area fraction was determined by the value required to attain convergence in the accumulated simulation results. In the simulations performed, a total of 200 bilayers has proved enough.

We also tested the effects of the finite size of the bilayer plane on the simulation results. It was verified that for a matrix whose dimensions were greater or equal to 6 times the diameter of the bleaching spot, the simulation results converged, within error, to the same values.

The fits between the simulated and experimental files were made by superposition of the experimental and the simulated results and "eye matching" the best fit.

Time-dependent recovery simulations

Within the context of the fixed-ellipse model, in each bilayer, numerically represented by the method already described, an analyzing spot with a radius of 3 μm is focused. The time-dependent recovery curves for a single bilayer plane are simulated by tracking the diffusion-limited random walk of a large number of probes in the area left free after the distribution of the nonpermeable ellipses and then computing the number of probes within the spot as a function of time. To decrease the number of probes that must be tracked, instead of following the diffusion of the unbleached fluorescent probes into the bleaching spot, we follow the diffusion of the bleached probes out of the spot. These two situations necessarily lead to the same results (as pointed out by Soumpasis, 1983), but the number of diffusing objects that must be considered is much reduced.

Each Monte Carlo run is parameterized by the fluid area fraction and the ellipse aspect ratio and size. For each combination of these parameters that, together with the model used, dictate the topology of the idealized bilayer, the simulation develops according to the following procedure.

Initial conditions

At zero time no unbleached probes reside inside the spot (100% bleaching efficiency), which is equivalent to saying that the fluorescence seen at the beginning is null, $F(t = 0) = 0$. For each simulated bilayer a number of tracers $N_B = 1000$, representing the bleached probes, is randomly dispersed in the fluid area inside the bleaching spot. Because we do not follow the diffusion of the nonbleached probes, we do not care about their number or position.

Diffusional jumps

All probe molecules are allowed to randomly jump to adjacent sites in a square lattice. One lattice site can be occupied by more than one molecule, but they cannot penetrate solid obstacles. In the case in which a step results in a tracer entering a solid domain, it will not move. A Monte Carlo step is concluded when all tracer molecules have attempted one jump in the lattice.

Time-dependent fluorescence

To determine the average for all possible domain patterns, the simulation is carried out for N_L independent bilayers and the results are summed. To compute the fluorescence intensity recovered at a given time, the probes still remaining inside the bleaching spot area in each bilayer are periodically counted. The sum for all bilayers at a given step s, denoted by $B(s)$,

can easily be converted into the number of unbleached probes inside the spot, $F(s)$:

$$F(s) = N_B N_L - B(s). \quad (4)$$

For the matrix resolution and dimension the requirements are different from those for the fractional recovery simulations. Whereas in the fractional recovery simulations, for the comparison of bleached and unbleached areas and inspection of their connectivity the only prerequisite is that the matrix resolution be such that the area of the defined ellipse is close to its analytical area; if we intend to simulate the time domain, other conditions must be considered to extrapolate the results from a random walk in a square lattice to a continuum.

Ideally, to simulate a time-dependent FRAP recovery curve by following the diffusion-limited random walk of a large number of trace molecules, a matrix resolution comparable to the molecular dimension in a bilayer should be used. It is not difficult to conclude that such a definition is neither practical nor necessary (300 Mb of random-access memory would be needed for the storage on a bit basis of a 40 × 40 μm bilayer sheet). To determine the optimal resolution, we based our work on the studies of the macroscopic diffusion of tracers on a obstructed triangular lattice by Saxton (1989). This author found that with nonoverlapping hexagonal obstacles with a radius of up to 16 lattice sites and for a given obstacle area fraction c, the macroscopic diffusion coefficient increases noticeably with the obstacle radius. For obstacles larger than 16 lattice sites, the macroscopic diffusion coefficient tends to a constant value, $(1 - c)D$, where D is the diffusion coefficient in a lattice free of obstacles. This means that for the same obstacle area fraction, obstacles with a dimension similar to the diffusing particle cause more relative hindrance to diffusion than bigger ones.

Based on the fractional recovery simulations, we conclude that the sizes of the obstacles are much greater than the dimensions of a phospholipid molecule (an ellipse with $a = 1$ μm and $b/a = 0.2$ will contain approximately 6×10^3 phospholipid molecules). Under such circumstances the molecular diffusion is, in practice, a continuum percolation problem, and the matrix resolution to be used is the one that allows the traces to view sufficiently large obstacles. For each fluid area fraction simulated, we tested the necessary resolution needed. As an example, in Fig. 2 *A* is represented the recovery simulated for different lattice resolutions for the fixed ellipse with $a = 1$ μm, $b/a = 0.3$, and $p = 0.52$. Above 16 lattice points per micron, no change in the time-dependent recovery curve is obtained. Lower resolutions are probably below the limiting condition referred to by Saxton, the ellipses being so small that they contribute to the diffusion hindrance, as can be deduced by the flatter curvature of the plot at initial times.

Two other aspects are relevant in defining the simulation conditions: the dimension of the simulation plane, and the number of bilayers and probes that must be averaged.

To avoid finite size effects, our simulations were performed using boundary conditions that force those trace molecules that reach the border of the bilayer plane to migrate from that side to the opposite one. In Fig. 2 *B*, for the same gel pattern, two simulations were carried out for two different bilayer plane dimensions. It was verified that, not only for the geometric patterns shown but for all of those explored in this work, the bilayer dimension must be at least equal to 6 times the diameter of the bleaching spot for the time-dependent curves to coincide.

The number of probes used per layer should be enough to describe, in a unique way, diffusion with percolation in that layer, and the number of layers observed must provide a sufficient averaging of gel pattern that differs from layer to layer. An acceptable noise and topology averaging procedure that constitutes a compromise between the noise level and the large computing time involved in these calculations has been found to be the use of 1000 trace molecules (bleached) per layer and 30 bilayers ($N_L = 30$). In Fig. 2 *C* is illustrated the progress of the simulation results so far, as a function of the number of bilayer planes accumulated.

To allow a comparison between the experimental and simulated curves obtained as described, the Monte Carlo steps, s, must be converted into real time, t, and both curves must be normalized.

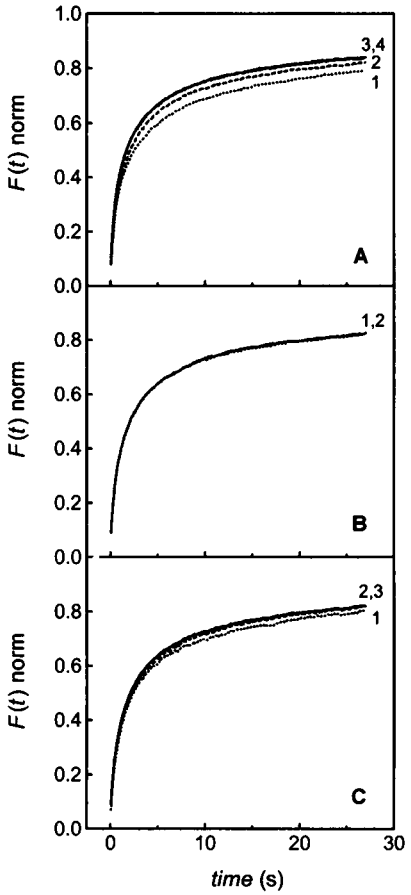

FIGURE 2 Tests for the time-dependent FRAP recovery curves obtained by Monte Carlo simulation. The plots are some examples of the tests that were done for the fixed-ellipse geometry model for a FRAP spot radius of 3 μm, solid ellipses having $a = 1$ μm, $b/a = 0.3$, and the fluid area fraction being $p = 0.52$. (*A*) Matrix resolution tests using the following resolutions: $r = 8$ points/μm (*curve 1*), $r = 12$ points/μm (*curve 2*), $r = 16$ points/μm (*curve 3*), and $r = 32$ points/μm (*curve 4*). All simulations were carried out with a bilayer plane dimension of 6 times the spot diameter, 1000 tracer molecules per layer, and 30 simulation layers. (*B*) Test of the dimension of the simulation plane using 6 times the FRAP spot diameter (6 × 2 × 3 μm = 36 μm) (*curve 1*) and 12 times the FRAP spot diameter (12 × 2 × 3 μm = 72 μm) (*curve 2*). Both curves were obtained with a matrix resolution of $r = 16$ points/μm, 1000 tracer molecules per layer, and 30 simulation layers. (*C*) Tests to define the number of simulated bilayers that should be averaged using 1000 tracer molecules per layer. With 10 layers (*curve 1*), 20 layers (*curve 2*), and 30 layers (*curve 3*). For all curves the matrix resolution is $r = 16$ points/μm, and the bilayer plane dimension is 6 times the spot diameter.

The conversion of steps in equivalent time is performed using Eq. 5, in which r is the imposed two-dimensional array resolution, which defines the length of the jumps made by the tracers in each step, and D is the probe diffusion coefficient, estimated for the temperature to which the simulation refers, by using an Arrhenius plot:

$$t = \frac{r^2}{4D} s. \quad (5)$$

Normalization of simulated and experimental curves is done according to

$$F(t)_N = \frac{F(t) - F(0)}{F(t < 0) - F(0)}. \quad (6)$$

In this equation $F(t)_N$ is the normalized fluorescence intensity at time t, and $F(t)$, $F(0)$, and $F(t < 0)$ are, respectively, the fluorescence intensity at t, fluorescence intensity at the beginning of the experiment/simulation, and fluorescence intensity before the bleaching step, all of them in arbitrary units.

The way in which $F(0)$ is obtained deserves further consideration. Whereas in our simulations $F(0) = 0$ because we impose a 100% bleaching efficiency, in a real FRAP experiment the fluorescence intensity at time 0 is not exactly known (because of the initial dead time, during which the shutter is closed to protect the photomultiplier from the intense bleaching beam). In homogeneous two-dimensional systems $F(0)$ is readily obtained from the fit of the FRAP curve to the usual Soumpasis law. In our phase-separated bilayers, however, we have to rely on some arbitrary mathematical law to rebuild the beginning of the recovery curve to retrieve $F(0)$. Because for the very initial recovery, where the diffusion of the probes neighboring the edge of the spot is observed, the Soumpasis equation should be valid, we have used the Soumpasis equation summed with a linear ramp to obtain a good fit and derive a credible value for $F(0)$ (Vaz et al., 1989, 1990; Bultmann et al., 1991; Almeida et al., 1992b).

The value of $F(t < 0)$ is $N_B \times N_L$ in the case of the simulations, whereas in the experimental FRAP data it is the average fluorescence intensity preceding the bleaching step, as already stated.

Because of the large computer time necessary to perform a single simulation, a recursive fitting routine optimizing the parameters involved is not practicable, and a simple "eye matching" fit was used to evaluate the goodness of fit.

Fluid-domain characterization

The fluid-domain counting and sizing are implicit when computing the expected fractional recovery by the Hoshen and Kopelman algorithm, and so, using the same kind of simulations, their size distribution was measured for given gel patterns near or below the percolation threshold.

RESULTS

Fractional recovery simulations

These simulations are intended to emulate the experimental fractional fluorescence recovery data as a function of temperature (or equivalent fluid fraction) for the system DMPC/DSPC with equimolar composition (Vaz et al., 1989).

Using the experimental fluorescence intensity before photobleaching, $F(t < 0)$, and the parameters retrieved from the fit as described in the Methods section, fluorescence intensity at infinite time after photobleaching, $F(\infty)$, and fluorescence of the bleached sample before recovery, $F(0)$, the fractional recovery, R, is calculated (Fig. 3). The diffusion of NBD-DLPE in the DMPC/DSPC 50/50 matrix below the solidus line is rather important, as may be concluded from the relatively high fractional fluorescence recovery observed. This excessive recovery may be ascribed to a difficult structural matching at the grain boundaries (Derzko and Jacobson, 1980). However, because of the almost exclusive solubility of the probe in the fluid phase, once there is fluid in the system, all of the NBD-DLPE will report only this phase. In this way we are for the moment mainly concerned with the data obtained for relatively large fluid fractions.

According to finite size scaling arguments given by the percolation theory (Stauffer and Aharony, 1994), Almeida et al. (1993) proposed an expression for the percolation

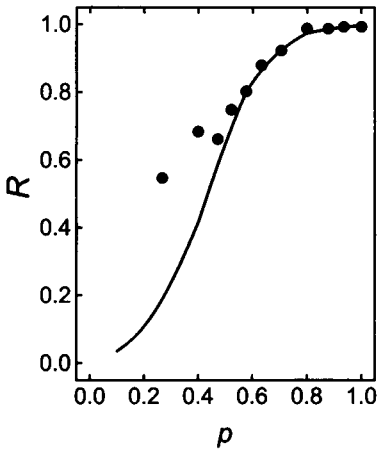

FIGURE 3 Experimental fluorescence fractional recovery plots obtained for the DMPC/DSPC (50/50) system (Vaz et al., 1989). The circles represent the experimental fractional recoveries (R) as function the fluid area fraction (p). The solid curve corresponds to the fit of Eq. 7 (see text) to the experimental R versus p. The parameters retrieved from the fit are the percolation threshold, $p_c = 0.44$, and the system linear dimension, $L = 3.98$.

probability, $P(p)$, of the liquid phase as a function of the area fraction of that phase, p:

$$P(p) = \frac{e^{AL^{1/\nu}(p-p_c)}}{1 + e^{AL^{1/\nu}(p-p_c)}}. \quad (7)$$

In this equation A is a constant equal to 3.5 (determined by Monte Carlo simulations), ν is a critical exponent with a value of 4/3 (Stauffer and Aharony, 1994), p_c is the percolation threshold, and L is the linear dimension of the system, which in a FRAP experiment is defined by the ratio ω/ϕ, where ω is the radius of the bleached spot and ϕ is the average characteristic length of the liquid domains (Almeida et al., 1993). Once fitted to the fractional recovery data, Eq. 7 makes it possible to obtain not only the system percolation threshold, p_c, corresponding to the sigmoid inflection point, but also ϕ, which is related to the steepness of the sigmoidal curve quantitatively associated with L. Because ϕ is a measure of the linear dimension of the system fluid domains, one can presume that it should also be conditioned by the solid domain dimensions.

The better fit of Eq. 7 to the experimental results in the high fluid fraction range, allowing both p_c and L to vary, provides a percolation threshold value of 0.44 and $L = 3.98$ μm (Fig. 3). Considering the fixed-ellipse gel-phase model and taking into account the relation between the percolation threshold and the aspect ratio of the elliptical solid domains, as calculated by Xia and Thorpe (1988), the value of b/a should be approximately 0.3, and from the value of L we can expect the linear average dimension of the fluid phase to be ~0.75 μm. The fit did not consider the experimental points at small fluid area fractions for the reason explained earlier.

Considering this b/a value estimate as a first approximation, we have simulated the fractional recovery plots as a

function of the fluid area fraction for different ellipse dimensions ranging from a equal to 100 nm up to 1.0 μm, and aspect ratios from 0.1 to 0.3. Some of the simulations that better approximate the experimental data are presented in Fig. 4. The best fit for the high fluid fraction range of the experimental curve leads to an ellipse semi-major axis of 1.0 μm with an aspect ratio equal to 0.2 (Fig. 4 *A*, *solid line*). It should be noted that the simulation results are highly dependent on the geometry of the system, being strongly conditioned by the gel phase model adopted. The results shown in Fig. 4 *B*, for example, show simulations with parameters identical to those used in Fig. 4 *A*, with the exception that the aspect ratio in Fig. 4 *B* is 0.3.

An illustrative example of the fixed-ellipse geometry model applied in these simulations can be found in Fig. 5, where three planes, representing the same bilayer sheet, are presented for three different fluid area fractions, above, at and below the system p_c. Whatever the fluid area fraction, the fluid domains will have a complex geometry as a result of the random placement of the elliptical solid domains imposed by the model.

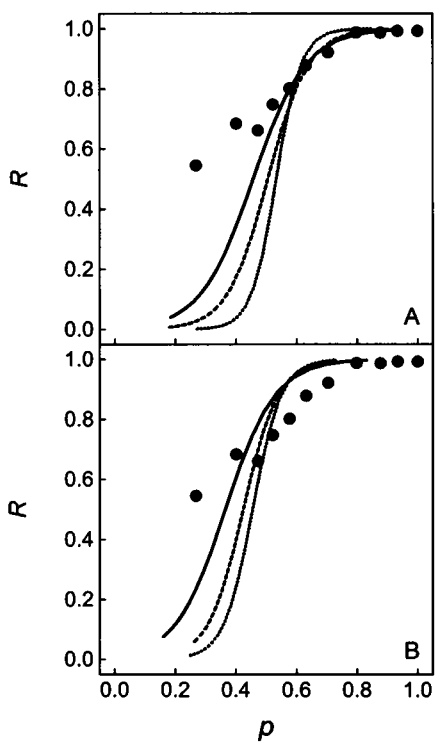

FIGURE 4 Simulation of the fluorescence fractional recovery plots obtained for the fixed-ellipse model for different geometries of the solid elliptical domains, demonstrating the sensitivity of the result on the values of the parameters. (*A*) Three outputs from the fractional recovery simulations, where the ellipse's b/a is equal to 0.2 and the semi-major axis a equals 0.25 μm (*dotted line*), 0.5 μm (*dashed line*), and 1.0 μm (*solid line*). (*B*) Same as *A*, but with b/a equal to 0.3. Simulation conditions: FRAP spot radius of 3 μm, matrix resolution r = 16 points/μm, and bilayer plane dimension 6 times the spot diameter. The circles represent the experimental values.

Time-dependent recovery simulations

We shall now consider our Monte Carlo simulations of experimental FRAP curves in the time regime for the system under examination. For these simulations we have assumed the solid-domain topology inferred from the former collection of simulations as a point of departure.

The fits to the fractional recovery, made in the conditions as described in the Methods section, for ellipses with a = 1 μm and b/a = 0.2, are definitely not acceptable, as shown on Fig. 6 (*series of curves numbered 2*). Poor fits are observed for fluid area fractions both above and below the system percolation threshold, which, according to Xia and Thorpe (1988) for an aspect ratio of 0.2, is 0.54. Keeping the semi-major axis size unchanged but increasing the aspect ratio to 0.3 results in a much better fit. As can also be seen in Fig. 6 (*series of curves numbered 1*), the model fits to the experimental data are reasonably good for the intermediate range of fluid fractions (p = 0.80–0.47). The correspondence between the experimental and simulated curves becomes quite unacceptable for small fluid fractions, particularly below the percolation threshold. Therefore, according to these time-resolved simulations, the best model fit leads to ellipses with an aspect ratio of 0.3 and not 0.2, as deduced from the fractional recovery at infinite time (see Fig. 4), for the same semi-major axis size of 1 μm. We should point out, however, that even with an aspect ratio of 0.3, comparison of the simulated curves with the experimental ones shows significant mismatches, particularly in the initial phase (see, for example, Fig. 6, *C* and *D*).

Simulations were also performed for several other geometries, with a ranging from 0.5 to 1.5 μm, and b/a from 0.2 to 0.4 (results not shown), but all values different from a = 1.0 $\pm$ 0.1 μm and a/b = 0.3 $\pm$ 0.02 led to a worst description of the experimental data.

An attempt was made to make the model more realistic, being fully aware that several scenarios are possible, to obtain an even better correspondence between the simulated and experimental curves. One such scenario could start with randomly dispersed and oriented crystallization seeds and allow the solid domains to grow in the direction of both axes at a rate inversely proportional to the linear dimension of the axis perpendicular to the growing direction. Although more complicated, this new growing ellipses model complies with the crystal growth theories (Markov, 1995) and is more consistent with what is observed in macroscopic systems. Moreover, because we allow the ellipses to superpose each other, from the diffusion point of view a dendritic-like structure will be obtained.

Two unknown variables are associated with the growing ellipses model: the number of ellipses that should be considered, and their initial geometry. Taking into account the fixed-ellipse geometry model fits, we postulated that at a fluid area fraction of p = 0.52 we should have the ellipses' number and geometry given by that model, i.e., ellipses with a = 1 μm and b/a = 0.3, ellipse density of 0.68 ellipses/μm^2, and positioning in the bilayer plane given by the

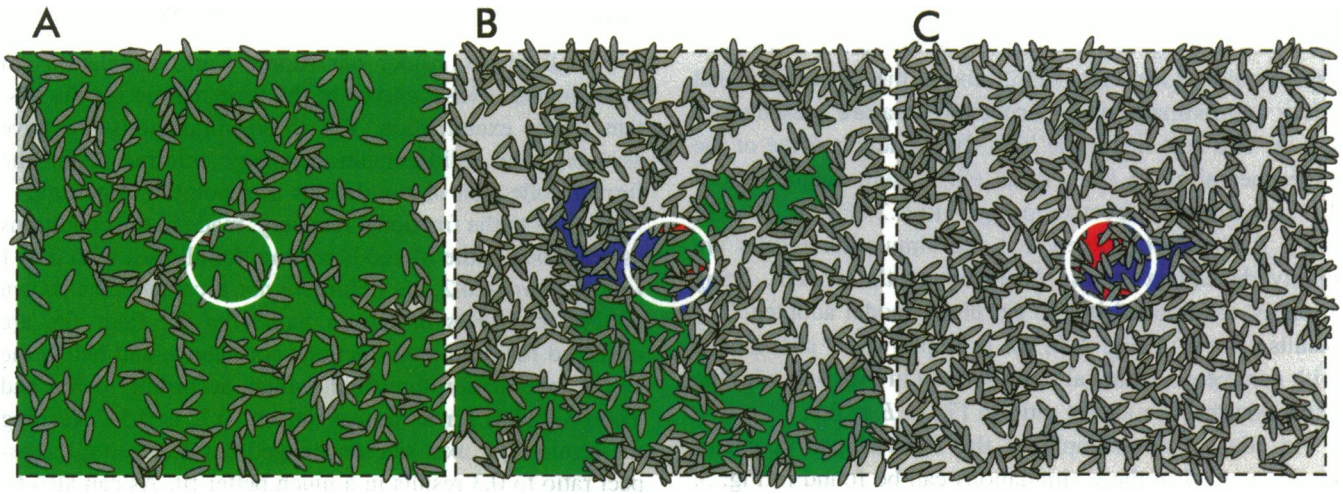

FIGURE 5 Single bilayer plane according to the fixed-ellipse geometry model for three different fluid area fractions: above (*A*), at (*B*), and below (*C*) the theoretical percolation threshold for the system, $p = 0.63$, 0.47, and 0.40, respectively. The solid domain units are represented by ellipses with $a = 1.0$ μm and $b/a = 0.3$; the spot radius, represented by the centered circle, is 3 μm; the matrix resolution $r = 16$ points/μm; and the side of the bilayer plane represented is 5 times the spot diameter. In all three figures the green area represents an "infinite" fluid domain that expands outside the simulation plane, the blue areas represent partially recoverable domains, and those painted red are totally unrecoverable domains that are inside the bleached circle. In this specific plane the fractional fluorescence recovery at equilibrium is 0.97 for *A*, 0.80 for *B*, and 0.40 for *C*.

simulation performed for that fluid area fraction. Although any other fluid area fraction could be chosen, we opted for $p = 0.52$, because within all fractions studied it was the one that led to the best fixed-ellipse model fit.

After fixing the gel characteristics for a given fluid area fraction, we attempted by trial and error to find out the constant ratio between the two ellipse axial growth rates that would lead to the best fit through the whole set of fluid fractions for which experimental data were available. The best result was obtained when the rate of growth in the direction of the ellipse minor axis was 90% of that for the major axis. Under this condition the growing ellipses become progressively thinner, beginning with $a = 0.42$ and $b/a = 0.43$, for $p = 0.80$, and ending, for $p = 0.40$, with $a = 1.29$ and $b/a = 0.25$.

The simulation outputs from the ellipse growing model, together with the correlated experimental results, are presented in Fig. 7. We now observe that the initial recovery, dominated by the diffusion of probes in the vicinity of the spot, is better simulated, but for long times there is no real improvement. For low fluid area fractions the disagreement between experiment and model continues to be significant.

Fluid-domain characterization

As a result of the random placement of the elliptical solid domains, the resulting fluid domains will obviously have an undefined geometry. Even though we could not characterize the fluid domains in terms of their geometry, we tried to describe them with respect to their mean size and size distribution. Using the same fractional recovery simulation applied to the fluid fractions of interest, it is possible to make the required calculations. It only makes sense to think about finite fluid-domain sizes if the system fluid fraction is below the percolation threshold ($p < p_c$), because above it there will always be at least one infinite fluid cluster.

Considering the fixed-ellipse geometry model and its best fit to the DMPC/DSPC (1:1) system, $a = 1$ μm and $b/a = 0.3$, we present in Fig. 8 the fluid domain histograms for four different fluid fractions, one above and three below the system percolation threshold ($p_c = 0.46$). In each plot we present a histogram of the fractional total fluid area occupied by domains as a function of their size. The histograms include all domains found.

Above, but near, the percolation threshold, at $p = 0.50$, although the majority of the domains are already very small (data not shown), the greatest contribution to the total fluid area is from very large fluid domains, where at least one should be a "infinite" cluster. In this case perhaps it does not make sense to retrieve a mean fluid domain area, because it will be strongly affected by domains that are not finite (in reality they are, but this is due, of course, to the finite size of the simulation plane).

Below, but still near, the percolation threshold, the fluid domain population is now more evenly distributed, and although infinite domains do not exist, we still have very large finite domains. For a fluid area fraction equal to 0.40, the mean fluid domain area obtained was 76 μm^2.

As the fluid area fraction is decreased, the size distributions of the fluid domains are progressively compressed toward smaller domain areas. The mean fluid domain areas calculated for the fluid fractions of 0.30 and 0.20 were 10 μm^2 and 2.5 μm^2, respectively.

DISCUSSION

As shown in the last section, the Monte Carlo simulations for fractional recovery and time-dependent recovery lead to

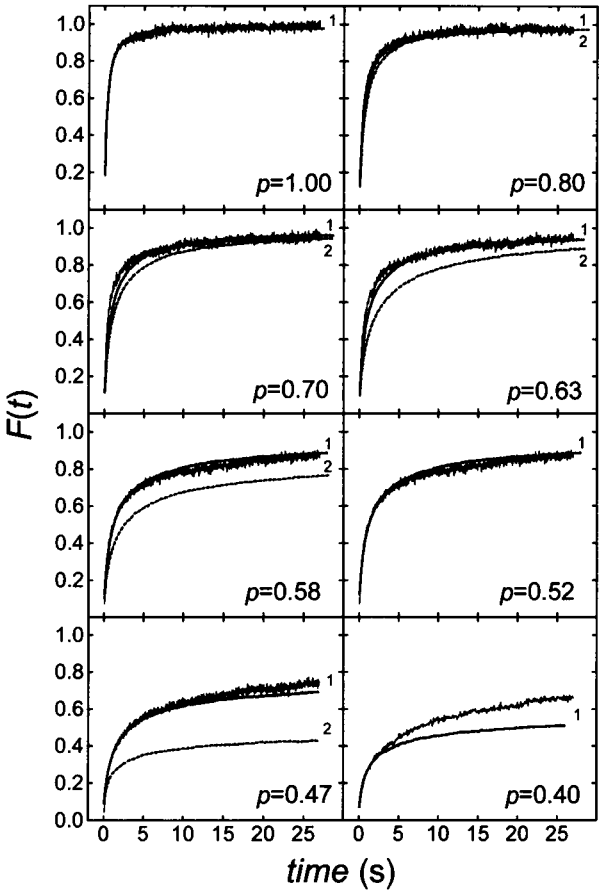

FIGURE 6 Time-dependent experimental fluorescence recovery curves obtained for the DMPC/DSPC (50/50) system (Vaz et al., 1989) for fluid area fractions, p = 1.00, 0.80, 0.70, 0.63, 0.58, 0.52, 0.47, and 0.40. The correlative recovery curves were calculated from Monte Carlo simulations considering the gel phase modeled by the fixed-ellipse model with a equal to 1.0 μm and two different values of b/a, 0.3 (*solid line, 1*) and 0.2 (*dashed line, 2*), corresponding to p_c = 0.54 and p_c = 0.46, respectively. All simulations were carried out for a spot radius of 3 μm, and with a matrix resolution of r = 16 points/μm, a bilayer plane dimension of 6 times the spot diameter, and average for 1000 tracer molecules per layer in 30 simulation layers.

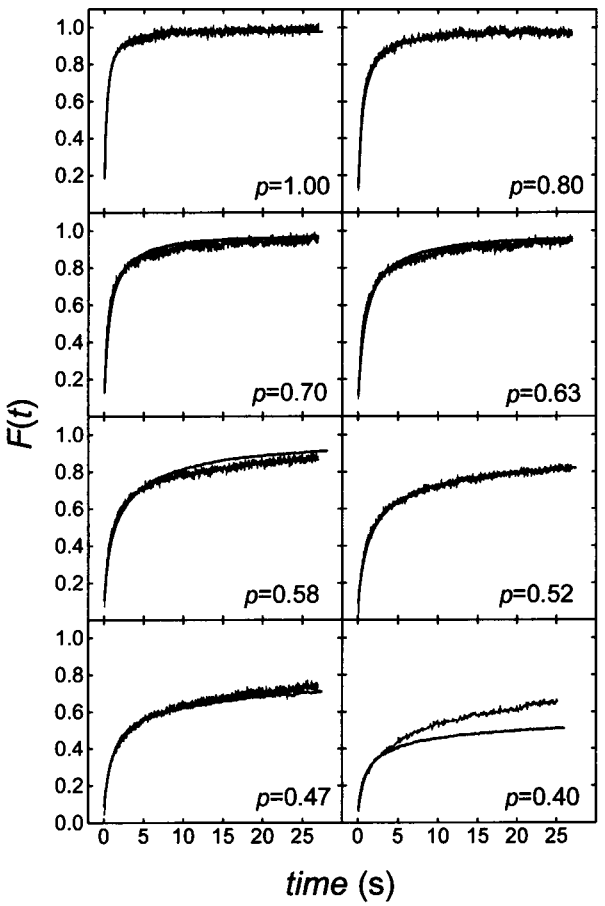

FIGURE 7 Time-dependent experimental fluorescence recovery curves obtained for the DMPC/DSPC (50/50) system (Vaz et al., 1989) at different fluid area fractions, and the corresponding ones as a result of Monte Carlo simulations. The model used assumes that the gel phase is constituted by a fixed number of growing ellipses (see text for details). The ellipse geometry, indicated below, was computed taking into account a constant ratio of axis growth rates, v_b/v_a, of 0.9. The fluid area fractions and solid-ellipse geometries represented are: p = 1.00; p = 0.80 where a = 0.42 and b/a = 0.43; p = 0.70 where a = 0.65 and b/a = 0.39; p = 0.63 where a = 0.77 and b/a = 0.36; p = 0.58 where a = 0.88 and b/a = 0.33; p = 0.52 where a = 1.0 and b/a = 0.3; p = 0.47 where a = 1.12 and b/a = 0.27; and p = 0.40 where a = 1.29 and b/a = 0.25. In all simulations the spot radius is 3 μm, the matrix resolution r = 16 points/μm, and the side of the plane is 6 times the spot diameter, with an average of 1000 tracer molecules per layer and 30 simulation layers.

different ellipse geometries, although the same topological gel model is used in both simulations. Furthermore, discrepancies with the results and methods of other authors must be analyzed.

If, according to the fixed-ellipse geometry model, the ellipse aspect ratio should effectively be 0.3, and not 0.2, why then the bad correlation between theory and experiment shown for the fractional recovery versus fluid area (Fig. 4 *B*)? The answer to this question is twofold. First, the fractional recovery deduced from the experimental FRAP curves in cases where a significant amount of solid phase exists are probably not simply describable by the Axelrod et al. (1976)/Soumpasis (1983) expressions. The analysis of these curves force-fitted the experimental fluorescence recovery process to a biphasic expression that assumed a rapid diffusional process superimposed upon a much slower recovery process that was simulated by a linear ramp (Vaz et al., 1989). The slow regime is due in fact to diffusion with percolation and diffusion of the tracer in gel-phase defects, and there is no way, from a simple curve-fitting analysis, to separate these two components. As shown by Saxton (1994), the global diffusion coefficient for diffusion with percolation is time dependent. In the limit of very short times, the diffusion coefficient obtained tends to the time-independent diffusion coefficient observed in a pure fluid phase. Thus the experimental curves contain, in fact, two types of diffusion processes that are physically distinct from each other, namely, diffusion with percolation and diffusion in gel-phase defects. The analysis of the experimental curves, therefore, produces an artificially reduced value of

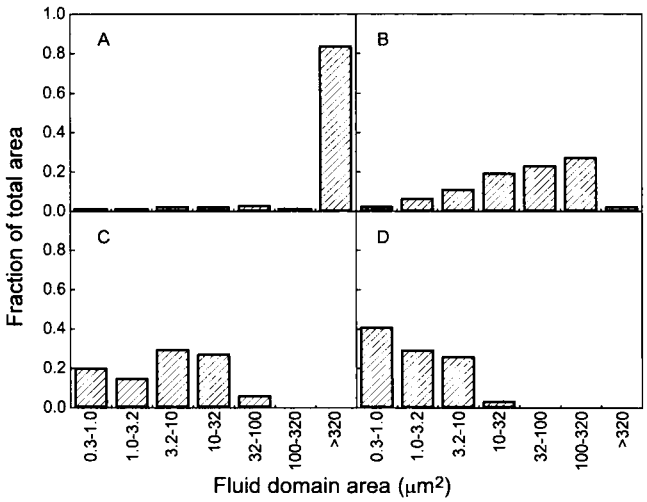

FIGURE 8 Fluid domain histograms characterizing the fixed-ellipse geometry model with a equal to 1.0 μm, b/a equal to 0.3 for four different fluid fractions, $p = 0.50$ (*plot A*), $p = 0.40$ (*plot B*), $p = 0.30$ (*plot C*), and $p = 0.20$ (*plot D*). The histograms represent the fraction of the total area of the simulated plane occupied by fluid domains as a function of the area of the individual fluid domains. The labels of the x axis, presented in a logaritmic progression, represent the range of domain areas corresponding to each column. Histogram *A* shows that practically all of the fluid in a membrane with $p = 0.50$ is in continuous domains larger than 320 μm^2 (domains cannot be larger than the fluid area of the simulated plane, 648 μm^2), whereas at $p = 0.20$ (*histogram D*), most of the fluid is dispersed in domains smaller than 10 μm^2 (total fluid area per layer is 259 μm^2). For the calculations, square planes with sides of 36 μm and a matrix resolution $r = 16$ points/μm were used. The mean fluid domain areas retrieved from the distributions shown were 577 μm^2 for $p = 0.50$, 76 μm^2 for $p = 0.40$, 10 μm^2 for $p = 0.30$, and 2.5 μm^2 for $p = 0.20$.

$F(\infty)$. Second, in the Monte-Carlo simulations in the time regime we are simulating real experimental data and not conclusions derived from them. In this process the Monte Carlo method exclusively simulates the diffusion with percolation, no other assumptions being made.

Neither the fixed-ellipse geometry nor the growing-ellipse model gives good fits to the time-dependent recovery data for low fluid area fractions. The initial recovery is well simulated, but for longer times, the experimentally observed recovery is much larger than the simulated one. Because DMPC (and, in particular, DMPC/DSPC (1:1)) mixtures show a large recovery in the pure gel phase, one can be led to think that the channels in the gel, because of crystalline structural mismatch (grain boundary defects), are so large that some of the recoveries seen in cases with low fluid area fractions are due to gel-phase diffusion. This fact would explain the large recoveries experimentally verified at long times. However, that cannot be the case, because the fluorescent probe used in the FRAP experiments partitions almost exclusively in the fluid phase, as demonstrated by fluorescence polarization (Vaz et al., 1989), and, consequently, even for very small fluid fractions, practically all of the observed probe is actually in a fluid environment. Thus we should seek another interpretation for the results obtained. Initially the fluorescence is recovered because of the diffusion of the probes present in fluid domains that are only partially bleached. Obviously our model accounts for this phenomenon, and the initial part of the curve is well simulated. Because the area of these domains is relatively small, their depletion is fast and the probe concentration rapidly becomes uniform. Afterward, probes from adjacent fluid pools are drained through the channels existing in the lines of connection between crystals. As we have already seen, there is a significant mismatch at the grain boundaries of these crystals, and very short channels created by tangent crystals, nonpermeable to the probe in the computation, may be quite easily bridged in the real membrane. The characteristic time constant for this process must be on the order of magnitude of those obtained for the gel-phase diffusion. Obviously this could also be simulated, but given the unknowns involved, the parameters obtained would hardly have any physical meaning. The most effective way to corroborate this explanation is to make a similar Monte Carlo analysis in a experimental system in which defect diffusion between the solid domains is not significant. Preliminary results with the LigGalCer/DPPC (1:4) system (Almeida et al., 1992b), where diffusion in the gel phase is much less pronounced, gives support to this interpretation.

To further confirm the legitimacy of our topological approach, the next obvious step would be to verify experimentally that the FRAP results for systems with phase coexistence are strongly dependent on the value of the spot radius, as our present results suggest. As an example, we present in Fig. 9 two time-dependent recovery simulations brought about in the same system with the fixed-ellipse geometry model, but with different spot radii. As intuitively expected, the recovery obtained with a smaller area of observation (spot radius equal to 1.5 μm) leads to a faster and more complete recovery. This evidence could be a valuable support of the phase models assumed, but again a system having negligible recovery in the gel phase would be more adequate.

In a recent paper Schram et al. (1994) studied the consequences of the presence of nonoverlapping circular obsta-

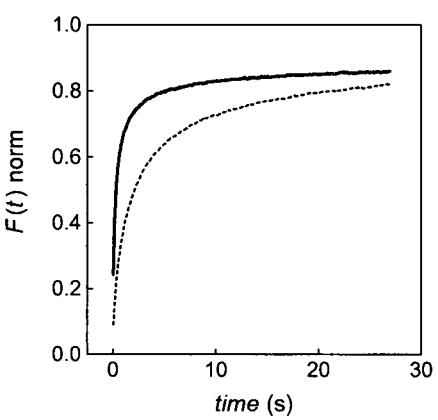

FIGURE 9 Comparison of the time-dependent recovery for two different FRAP spot radii. The dashed line is obtained in the same conditions as in plot F of Fig. 6, that is, with a spot radius of 3 μm, whereas the fluorescence recovery represented by the solid line was simulated for the same bilayer topology, but with a spot of 1.5 μm.

cles in the membrane by Monte Carlo simulation of FRAP experiments. Their results clash with ours, because in our case we confirm both from experiment and simulation the predictions of the percolation theory (Stauffer and Aharony, 1994; Saxton, 1994), namely, that the diffusion coefficient in a percolating two-dimensional system is time dependent, and we are led to conclude that either because of lack of resolution of the simulations performed or because the obstacles in their experimental systems are not allowed to overlap, they were not studying a percolating system in the sense that we use the term here.

Using IR spectroscopy, Mendelson et al. (1995) detected domains of one to 100 molecules, the maximum domain size detectable with the technique used.

The dimensions of the fluid clusters estimated by Sankaram et al. (1992) are much smaller (~5 orders of magnitude smaller) than those obtained from FRAP simulations and seem inconsistent with these. We suggest that the size of fluid domains proposed by these authors is somehow limited by the technique used. In fact, if the fluid domains in the DMPC/DSPC (1:1) system studied by these authors indeed had dimensions of just 100 nm^2, the fluorescence recovery in the FRAP curves should have dropped abruptly at the percolation threshold (Almeida, 1992), which was clearly not the case (Vaz et al., 1989; Vaz et al., 1990; Bultmann et al., 1991; Almeida et al., 1992a,b, 1993).

This work was supported by JNICT contract PBIC/CEN/1088/92. FPC is indebted to JNICT-Portugal for grant BD/349/93.

REFERENCES

Almeida, P. F. F. 1992. Lateral diffusion and percolation in two-phase lipid bilayers. Ph.D. thesis. University of Virginia. 54–71.

Almeida, P. F. F., W. L. C. Vaz, and T. E. Thompson. 1992a. Lateral diffusion in the liquid phases of DMPC/cholesterol lipid bilayers: a free volume analysis. *Biochemistry.* 31:6739–6747.

Almeida, P. F. F., W. L. C. Vaz, and T. E. Thompson. 1992b. Lateral diffusion and percolation in two-phase two-component lipid bilayers. Topology of the solid phase domains in plane and across the lipid bilayer. *Biochemistry.* 31:7198–7210.

Almeida, P. F. F., W. L. C. Vaz, and T. E. Thompson. 1993. Percolation and diffusion in three-component lipid bilayers: effect of cholesterol on an equimolar mixture of two phosphocholines. *Biophys. J.* 64:399–412.

Axelrod, D., D. E. Koppel, J. Schlessinger, E. Elson, W. W. Webb. 1976. Mobility measurement by analysis of fluorescence photobleaching recovery kinetics. *Biophys. J.* 16:1055–1069.

Bultmann, T., W. L. C. Vaz, E. C. C. Melo, R. B. Sisk, and T. E. Thompson. 1991. Fluid phase connectivity and translational diffusion in a eutetic two-comonent, two-phase phosphatidylcholine bilayer. *Biochemistry.* 30:5573–5579.

Derzko, Z., and K. Jacobson. 1980. Comparative lateral diffusion of fluorescent lipid analogues in phospholipid multilayers. *Biochemistry.* 19:6050–6057.

Hui, S. W. 1981. Geometry of phase-separated domains in phospholipid bilayers by diffraction-contrast electron microscopy. *Biophys. J.* 34: 383–395.

Hwang, J., L. K. Tamm, C. Böhm, T. S. Ramalingam, E. Betzig, and M. Edidin. 1995. Nanoscale complexity of phospholipid monolayers investigated by near-field scanning optical microscopy. *Science.* 270: 610–614.

Keller, D. J., J. P. Korb, and H. M. McConnell. 1987. Theory of shape transitions in two-dimensional phospholipid domains. *J. Phys. Chem.* 91:6417–6422.

Knoll, W., K. Ibel, and E. Sackmann. 1981. Small-angle neutron scattering study of lipid phase diagrams by the contrast variation method. *Biochemistry.* 20:6379–6383.

Luna, E. J., and H. M. McConnell. 1978. Multiple phase equilibria in binary mixtures of phospholipids. *Biochim. Biophys. Acta.* 509:462–473.

Mabrey, S., and J. M. Sturtevant. 1976. Investigation of phase transitions of lipids and lipid mixtures by high sensitivity differential scanning calorimetry. *Proc. Natl. Acad. Sci. USA.* 73:3862–3866.

Markov, I. V. 1995. Crystal growth for beginners. *In* Fundamentals of Nucleation, Crystal Growth, and Epitaxy. World Scientific Publishing Co. Pte., Singapore. 192.

Melo, E. C. C., I. M. G. Lourtie, M. B. Sankaram, T. E. Thompson, and W. L. C. Vaz. 1992. Effects of domain connection and disconnection on the yields of in-plane bimolecular reactions in membranes. *Biophys. J.* 63:1506–1512.

Mendelsohn, R., G. L. Liang, H. L. Strauss, and R. G. Snyder. 1995. IR spectroscopic determination of gel state miscibility in long-chain phosphatidylcholine mixtures. *Biophys. J.* 69:1987–1998.

Mouritsen, O. G., and K. Jørgensen. 1994. Dynamical order and disorder in lipid bilayers. *Chem. Phys. Lipids.* 73:3–25.

Press, W. H., B. P. Flannery, S. A. Teukolsky, and W. T. Vetterling. 1989. Numerical Recipes (Fortran Version). Cambridge University Press, Cambridge.

Radmacher, M., R. W. Tillmann, M. Fritz, and H. E. Gaub. 1992. From molecules to cells: imaging soft samples with the atomic force microscope. *Science.* 257:1900–1905.

Sankaram, M. B., D. Marsh, and T. E. Thompson. 1992. Determination of fluid and gel domain sizes in two-component, two-phase bipid bilayers. An electron spin resonance spin label study. *Biophys. J.* 63:340–349.

Saxton, M. J. 1987. Lateral diffusion in an archipelago. The effect of mobile obstacles. *Biophys. J.* 52:989–997.

Saxton, M. J. 1989. Lateral diffusion in an archipelago. *Biophys. J.* 56: 615–622.

Saxton, M. J. 1994. Anomalous diffusion due to obstacles: a Monte Carlo study. *Biophys. J.* 66:394–401.

Schram, V., J. F. Tocanne, and A. Lopez. 1994. Influence of obstacles on lipid lateral diffusion: computer simulation of FRAP experiments and aplication to proteoliposomes and biomembranes. *Eur. Biophys. J.* 23: 337–348.

Shimshick, E. J., and H. M. McConnell. 1973. Lateral phase separation in phospholipid membranes. *Biochemistry.* 12:2351–2360.

Snyder, R. G., H. L. Strauss, and D. A. Cates. 1995. Detection and measurement of microaggregation in binary mixtures of esters and of phospholipid dispersions. *J. Phys. Chem.* 99:8432–8439.

Soumpasis, D. M. 1983. Theoretical analysis of fluorescence photobleaching recovery experiments. *Biophys. J.* 41:95–97.

Stauffer, D., and A. Aharony. 1994. Introduction to Percolation Theory. Taylor and Francis, London.

Vaz, W. L. C. 1992. Translational diffusion in phase separated lipid bilayer membranes. *Comm. Mol. Cell. Biophys.* 8:17–36.

Vaz, W. L. C. 1996. Consequences of phase separations in membranes. *In* Handbook of Non-Medical Applications of Liposomes, Vol. 2. Y. Barenholz and D. D. Lasic, editors. CRC Press, Boca Raton, FL. 51–60.

Vaz, W. L. C., and P. F. F. Almeida. 1993. Phase topology and percolation in multi-phase lipid bilayer membranes: is the biological membrane a domain mosaic? *Curr. Opin. Struct. Biol.* 3:482–488.

Vaz, W. L. C., E. C. C. Melo, and T. E. Thompson. 1989. Translational diffusion and fluid domain connectivity in a two component, two-phase phospholipid bilayer. *Biophys. J.* 56:869–876.

Vaz, W. L. C., E. C. C. Melo, and T. E. Thompson. 1990. Fluid phase connectivity in an isomorphous, two-component, two-phase phosphatidylcholine bilayer. *Biophys. J.* 58:273–275.

Wiener, M. C., R. M. Suter, and J. Nagle. 1989. Structure of the fully hydrated gel phase of dipalmitoylphosphatidylcholine. *Biophys. J.* 55: 315–325.

Wu, S. H., and H. M. McConnell. 1975. Phase separation in phospholipid membranes. *Biochemistry.* 14:847–854.

Xia, W., and M. F. Thorpe. 1988. Percolation properties of random ellipses. *Phys. Rev. A.* 38:2650–2656.